Aust. J. Mar. Freshwater Res., 1988, **39**, 697–707

Comparisons between Surface, Barotropic and Abyssal Flows during the Passage of a Warm-core Ring

P. J. Mulhearn,[A] *J. H. Filloux,*[B] *F. E. M. Lilley,*[C] *N. L. Bindoff*[C,D] *and I. J. Ferguson*[C,E]

[A] Maritime Systems Division, Weapons Systems Research Laboratory, Defence Science and Technology Organisation, P.O. Box 706, Darlinghurst, N.S.W. 2010.
[B] Scripps Institution of Oceanography, University of California, San Diego, La Jolla, California 92093, U.S.A.
[C] Research School of Earth Sciences, Australian National University, G.P.O. Box 4, Canberra, A.C.T. 2601.
[D] Present address: Department of Earth, Atmospheric and Planetary Sciences, M.I.T., Cambridge, Mass. 02139, U.S.A.
[E] Present address: Department of Physics, University of Toronto, Toronto, Ontario M5S 1A7, Canada.

Abstract

A comparison is made of results for barotropic, surface and abyssal flows during the formation and passage of a warm-core ring in the East Australian Current. The barotropic velocities are estimated from sea-floor measurements of the horizontal electric field, which is induced by water motion. Values for the surface and near-bottom velocities are obtained generally by more traditional methods. A strong similarity is observed between the directions of the barotropic and surface flows. At a site close to the foot of the continental slope, the barotropic and near-bottom velocities are also similar, both in direction and magnitude. A possible explanation for this effect is that proximity to the coast constrains flow directions and causes the streamlines at depth to converge on the western (or near-shore) side of the warm-core ring.

The determination of barotropic velocities enables barotropic volume transports to be estimated and compared with traditional geostrophic volume transports calculated for water motion between the surface and a depth of 1300 m. The barotropic transports are found to be greater than the geostrophic transports by a factor of approximately 1·6, indicating the significance of deep-water flow in the East Australian Current.

Introduction

The East Australian Current, the western boundary current of the South Pacific Ocean, has been investigated over many years using hydrological and bathythermal data from ship cruises; see, for example, Hamon (1965), Andrews and Scully-Power (1976), Godfrey *et al.* (1980), Boland and Church (1981), Nilsson and Cresswell (1981) and Cresswell and Legeckis (1986). Such studies have concluded that eddies or warm-core rings form about twice a year adjacent to the coast from meanders in the East Australian Current. Some eddies coalesce again with the East Australian Current and do not escape to the south.

Most estimates of transport in the East Australian Current have been based on the application of the geostrophic equation to data from hydrology stations, with zero flow assumed at a particular reference level (commonly taken as 1300 m). Flow below the reference level is ignored. However, Boland and Hamon (1970) and Hamon (1970) used both hydrology stations and Swallow floats to measure absolute velocities, and from their results absolute transport estimates may be obtained. Thus, for a location near 33°15′S.,153°30′E., the absolute transport values (per km width of current) obtained from their data are

0067-1940/88/060697$03.00

$0{\cdot}77 \times 10^6$ m^3 s^{-1} and $1{\cdot}32 \times 10^6$ m^3 s^{-1} over the full water depth, compared with geostrophic values of $0{\cdot}62 \times 10^6$ m^3 s^{-1} and $0{\cdot}57 \times 10^6$ m^3 s^{-1} between 0 and 1300 m depth. At another location, near 32°S.,154°E., zonal transport over the full water depth is $0{\cdot}61 \times 10^6$ m^3 s^{-1}, compared with $0{\cdot}13 \times 10^6$ m^3 s^{-1} between 0 and 1300 m depth; corresponding meridional transport values are $0{\cdot}35 \times 10^6$ m^3 s^{-1} and $0{\cdot}17 \times 10^6$ m^3 s^{-1}, respectively. The data of Boland and Hamon (1970) and Hamon (1970) thus lead to barotropic/geostrophic flow ratios in a range 1·2 to 5, indicating significant departures in the measured flows from the geostrophic estimates.

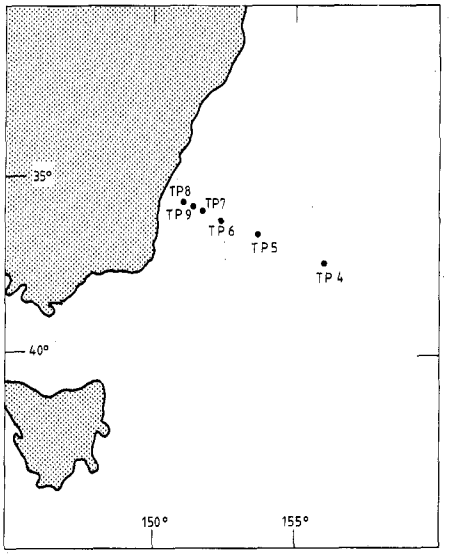

Fig. 1. Positions of sea-floor sites in the Tasman Sea relevant to the present paper.

Table 1. Sea-floor instruments contributing data for comparisons between surface, barotropic and abyssal flows during the passage of a warm-core ring

Site TP9 also included other instruments at 35°55′S.,151°22′E. At TP8, instrument recorded true north component only of horizontal electric field (giving east component only of barotropic flow)

Site No.	Latitude (S.)	Longitude (E.)	Depth (m)	Time span of data	Duration of data (days)	Instruments at site
TP4	37°33′	155°58′	4460	12.xii.83–9.ii.84	58	H
TP5	36°43′	153°35′	4660	25.i.84–27.iii.84	62	H
TP6	36°14′	152°15′	4836	15.xii.83–27.iii.84	103	H, V
TP7	36°00′	151°36′	4840	14.xii.83–26.iii.84	103	H
TP9	35°54′	151°23′	4850	14.xii.83–21.iii.84	98	R
TP8	35°49′	151°08′	4850	15.xii.83–26.iii.84	102	H (east only)

H, Horizontal electric field instrument; V, Vertical electric field instrument; R, Aanderaa recording current meter, 100 m above sea floor.

The present paper compares various measurements of surface, barotropic and abyssal flows made in the East Australian Current between December 1983 and March 1984, during the Tasman Project of Seafloor Magnetotelluric Exploration. This experiment, with both solid-earth and oceanographic objectives, involved a series of geophysical instruments placed at sea-floor sites in a line across the Tasman Sea, and continued inland on the Australian continent (Ferguson *et al.* 1985; Filloux *et al.* 1985; Lilley *et al.* 1986*b*). Figure 1 shows the recording sites which are relevant to the present paper, and Table 1 gives instrumental and

other details concerning them. The deployment of a current meter near the sea-floor at site TP9 introduced long-term abyssal current-meter measurements to the East Australian Current, and provided new and valuable information on the deep flow.

During the recording period, a meander of the East Australian Current moved south over the line of instruments and pinched off to form a warm-core ring, which continued to drift southward. The ocean currents associated with this phenomenon gave rise to long-period signals of the sea-floor horizontal electric field (HEF) which were unusually strong, and which (as reported by Lilley *et al.* 1986*a*) can be used to estimate depth-averaged (barotropic) velocities at each of the HEF instrument sites.

In the present paper such barotropic results are compared with the near-surface and abyssal flows described by Mulhearn *et al.* (1986). Volume transport estimates, based on the barotropic velocity measurements, are then compared with traditional geostrophic results. In summary, the present paper ties together surface and abyssal information (Bindoff *et al.* 1986; Mulhearn *et al.* 1986) with barotropic information (Lilley *et al.* 1986*a*), and adds a comparison of barotropic and geostrophic volume transport estimates.

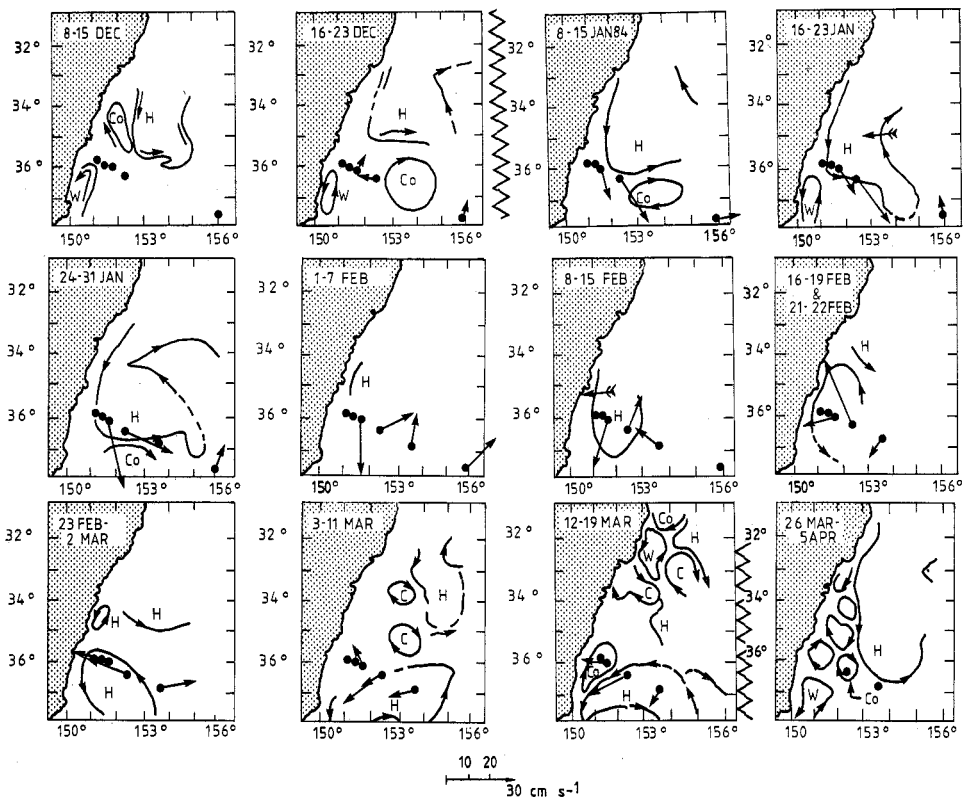

Fig. 2. Charts of positions of mesoscale surface features for time-spans of approximately 8 days from December 1983 to early April 1984. The positions of the Tasman Front and developing warm-core ring are indicated by the longer dark line in each box. Sea-floor measurement sites are shown by black dots when they were recording, and arrows emanating from them indicate barotropic velocity vectors (to scale shown). Other arrows (not to scale) indicate surface flow directions. Co indicates a cold-core eddy with T_{250} (temperature at 250 m depth) less than 16°; H indicates a region of T_{250} greater than 16°; C represents a region cooler and W a region warmer than its surroundings. Arrows ←←← indicate direction of movement of a feature over an 8-day charting interval. Note lack of data between 23 December and 8 January, and between 19 and 26 March.

Instruments and Methods

The sources of data, instruments and methods forming the basis of the comparisons of the present paper are described in detail in the contributing papers mentioned in the previous paragraph. For completeness a summary is now given.

Surface and near-surface observations of the East Australian Current consisted of aircraft-deployed bathythermographs (AXBTs), satellite-tracked buoy positions, infra-red satellite imagery, and various ship observations: ship-sets, sea-surface temperatures, and temperature profiles from expendable bathythermographs (XBTs) (Mulhearn *et al.* 1986). These data were collated into charts, corresponding approximately to weekly intervals of the recording period, which show the positions of thermal fronts at the edges of the East Australian Current, and the development of a warm-core ring. A series of such charts is shown in Fig. 2. A recording current meter measured the velocity of the abyssal flow at site TP9 (Mulhearn *et al.* 1986), and at site TP6 a vertical electric field instrument provided information on the magnetic-east component of the velocity near the sea floor (Bindoff *et al.* 1986).

The estimates of barotropic velocity, central to the present comparisons, originate from sea-floor measurements of the horizontal electric field using instruments described by Filloux (1980). The estimates are calculated as described by Lilley *et al.* (1986*a*), and rely on a number of factors:

(*i*) the horizontal length-scale of the water motion should be large compared with ocean depth;

(*ii*) the ratio of the vertical electrical conductance of the material beneath the sea floor (integrated from the bottom of the ocean down to the depth where leakage electric currents are zero) to the vertical electrical conductance of the ocean water should be small (the present barotropic velocities are based on an estimated value for this ratio of 0·1); and

(*iii*) departures from uniform electrical conductivity in the ocean column should be small, otherwise the barotropic velocities become weighted by the velocities where the electrical conductivity is highest. For the present case, where both mesoscale currents and sea-water electrical conductivity are expected to be strongest in the uppermost part of the water column, the barotropic velocities could be overestimated by perhaps 10%.

Velocity Comparisons

The vectors of weekly-average barotropic velocity included in Fig. 2 allow the following comparison of barotropic and near-surface flows.

The barotropic velocities at sites TP6 and TP7 are strong (greater than 15 cm s^{-1}) from the week 8–15 January 1984 onwards. They are usually similar in direction to the surface flows associated with the meander or ring, but up to mid February they tend to be directed outwards from the meander. In the period 16–22 February the barotropic velocities at TP6 and TP7 are large and appear not to be related to directions of surface fronts. This period was one of rapid transition shortly after ring pinch-off, when the ring moved on shore and then rapidly southwards. After 23 February the direction of the barotropic current again agrees with the direction of the surface current.

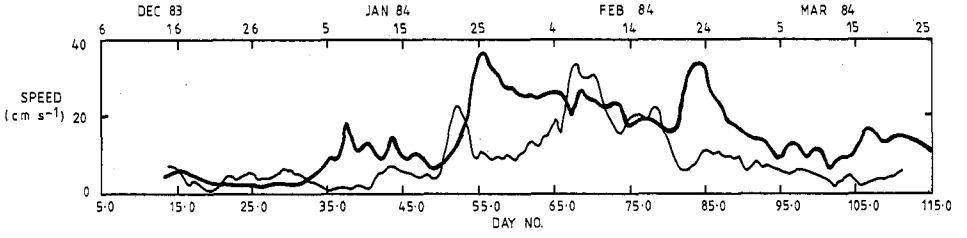

Fig. 3. Records of daily averages of abyssal speed at site TP9 (light line) and barotropic speed at site TP7 (heavy line).

The daily average speeds of the barotropic current at site TP7 and the abyssal current (100 m above the sea floor) at site TP9 are compared in Fig. 3. The two sites are 22 km apart, but Fig. 2 indicates that this distance is small compared with the scale of the warm-

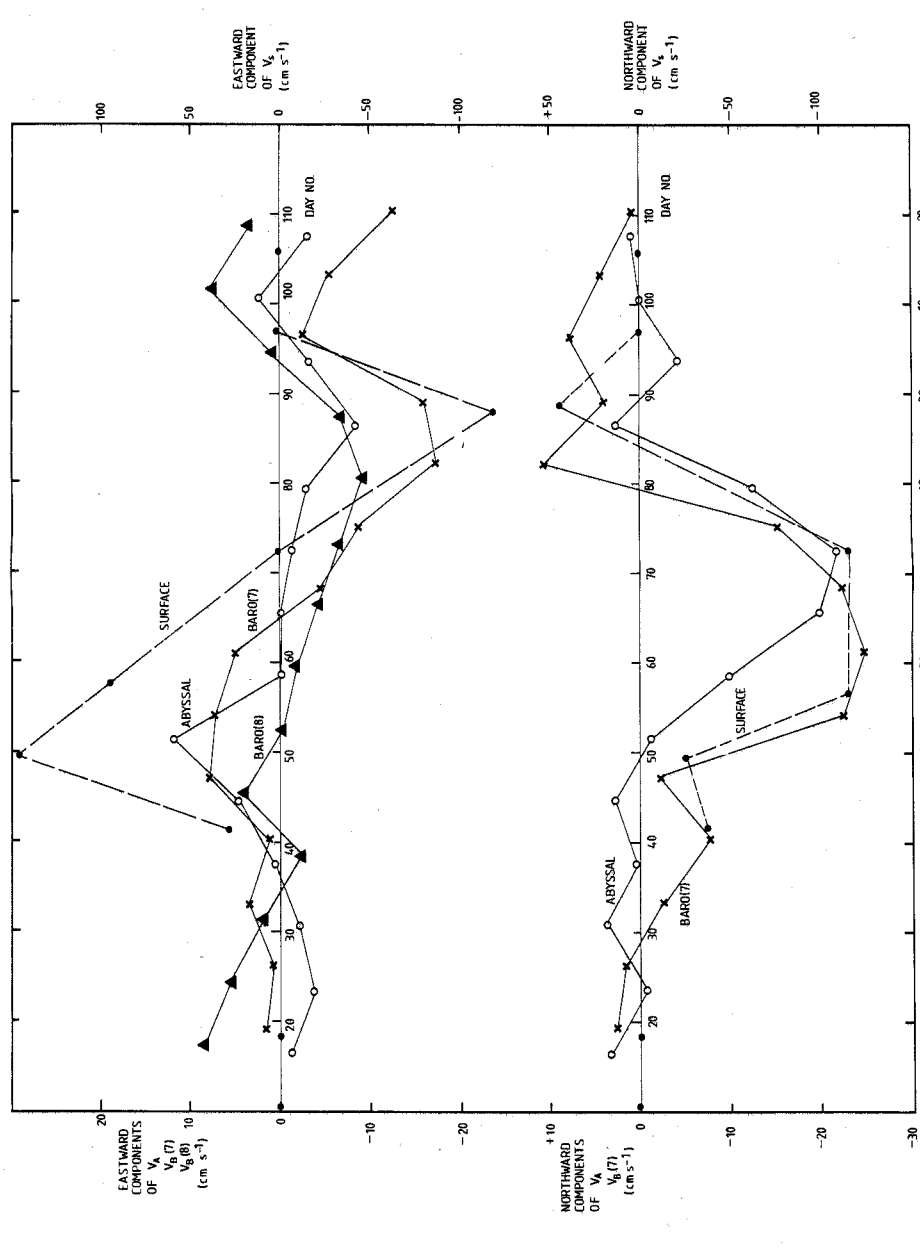

Fig. 4. Comparisons between barotropic, abyssal and surface velocity components at site TP7, TP8 and TP9: ● V_S, surface velocity at site TP7; ○ V_A, abyssal velocity at site TP9; × $V_B(7)$, barotropic velocity at site TP7; ▲ $V_B(8)$, barotropic velocity at site TP8 (eastward component only). Surface values are estimated from available data in each week; other values are weekly averages. Surface velocity data are plotted to a different vertical scale.

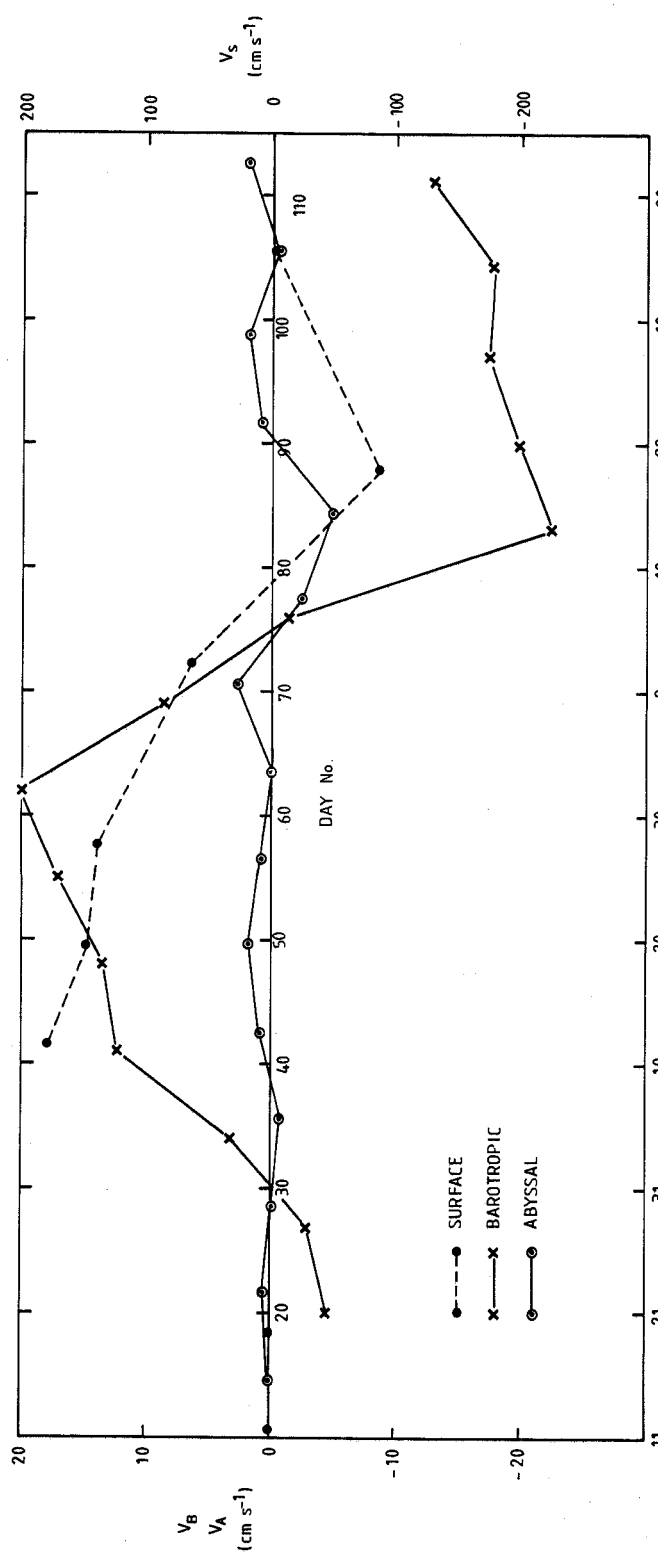

Fig. 5. Comparisons between eastward components of velocities at site TP6: V_S, surface velocity; V_B, barotropic velocity; V_A, abyssal velocity. scale for surface velocity data.

core ring. It can be seen that both currents increased markedly after 20 January, near the time at which the front reached the line of sea-floor sites. The most striking feature of Fig. 3 is that the barotropic and abyssal currents are of comparable magnitude, with the abyssal current at times being the larger of the two.

In Fig. 4 the weekly-average north and east components of the barotropic current at site TP7 are compared with those of the abyssal current at site TP9, the surface current at site TP7 (note different scale of plot), and the eastward barotropic current at site TP8. Site TP8, close to the foot of the continental slope at the western boundary of the abyssal plain, is 47 km from site TP7 and 78 km from the east Australian coast.

The north–south components for all sites in Fig. 4 have very similar behaviour, their strongest feature being a sustained flow to the south from about 20 January to 20 February (identifiable in the appropriate maps of Fig. 2). The east–west components in Fig. 4 are less similar, though all recordings have the same basic form; a sharp rise in eastward velocity after 10 January followed by a decrease to a maximum westward component around 25 February, and then another increase to the east. The simplest physical interpretation of the patterns observed is that the effects of the warm-core ring extend to the sea floor at these sites near the continental slope.

The weekly-average barotropic, abyssal and surface flows can also be compared further east at site TP6, 109 km away. This comparison is made in Fig. 5 (again note the different scale for the surface data) for the available east component. The surface and barotropic velocities are reasonably similar but show little correlation with the abyssal flow, except that all three show a westwards increase towards the end of February. It should be noted that the estimates of abyssal speed, from a vertical electric-field instrument, may be reduced by the effect of reduced water speed in a benthic boundary layer. The higher correlation between abyssal and barotropic velocities at TP7–TP9 compared with that at TP6 may be caused by convergence of streamlines on the western side of the warm-core ring as it pushes against the continental slope.

There is some evidence from Fig. 4 that the surface speed tends to be five times larger than the barotropic speed. The surface velocities associated with the warm-core ring are large and, as shown in Figs 4 and 5, often exceed 50 cm s^{-1}. Such surface speeds will contribute significantly to barotropic speed, and so the two would be expected to be closely related; however, a limitation in the present exercise may be that surface speeds are determined with relatively poor accuracy.

It is instructive to examine the surface and barotropic currents for any relative time lag between the occurrence of particular events. Figures 4 and 5 indicate that there is no significant (greater than one week) lag of barotropic events behind surface events. Close examination of the data in fact suggests that changes in the direction of surface flow and maxima of eastward and westward flow tend to occur a few days after the corresponding changes in the barotropic flow. Because of the sparsity of surface data and the limited accuracy of surface flow-speed estimates, it is not possible, however, to make definite conclusions regarding time lags.

A final useful observation is that of the similarity between the eastward components of barotropic velocity at sites TP7 and TP8, also shown in Fig. 4. This similarity is interpreted as showing that the scale size of gross features of the warm-core ring is at least 50 km.

Conclusions to be drawn from the above velocity comparisons are the following.

(*i*) At sites near the coast the structure of the warm-core ring extends to the sea floor. This result is interpreted as being caused by a convergence of streamlines near the continental slope. The observed effect is less, further away from the continental shelf.

(*ii*) The surface and barotropic flow directions are generally similar, as expected considering the large contribution of the former to the latter.

(*iii*) The horizontal scale size of larger-scale structures of the warm-core ring is at least 50 km.

Volume Transport Estimates

In this section estimates of barotropic volume transport, based on the sea-floor horizontal electric-field data and the width of the current stream obtained from surface current observations, will be compared with corresponding estimates made by the geostrophic method. Attention will focus on the flow around the meander described above and in Fig. 2. The geostrophic method will assume a level of no motion at depth 1300 m.

The geostrophic transport estimates will employ temperature data from XBT, AXBT and CTD observations, and will use the relationship (converted to S.I. units) of Andrews *et al.* (1980), that

$$G = 2{\cdot}8 \times 10^6 \Delta\Phi/\sin\theta \qquad (1)$$

In this equation, G denotes the geostrophic volume transport in $m^3\ s^{-1}$ between two sites which have a difference in geopotential anomaly of $\Delta\Phi$ (in $J\ kg^{-1}$). The relationship is for geostrophic flow between the surface and depth 1300 m, and is based on a 'universal' velocity profile in the East Australian Current. Geographic latitude is denoted by θ.

Values of $\Delta\Phi$ are calculated by applying observed temperature data to the regression equation (converted to S.I. units) of Pearce (1983):

$$\Phi(0/1300) = 4{\cdot}56 + 0{\cdot}926\,T_{250} \qquad (2)$$

where $\Phi(0/1300)$ denotes the geopotential anomaly (in $J\ kg^{-1}$) between the surface and 1300 m depth, and T_{250} denotes the temperature at 250 m depth. This equation is estimated to have an r.m.s. accuracy of 0·7 to 0·8 $J\ kg^{-1}$. Thus, if two stations have a temperature difference of ΔT_{250} at depth 250 m, equation (2) applied to each leads to

$$\Delta\Phi = 0{\cdot}926\,\Delta T_{250} \qquad (3)$$

with a r.m.s. accuracy of approximately $\pm 1{\cdot}1\ J\ kg^{-1}$, assuming uncorrelated data. However much of the subsurface structure at the two sections will be similar, so that the r.m.s. accuracy would be between 0·75 and 1·1 $J\ kg^{-1}$. Equation (3) may be substituted in equation (1) to determine G to an r.m.s. accuracy of $3{\cdot}5 \times 10^6$ to $5 \times 10^6\ m^3\ s^{-1}$. The latitude value taken for the present determinations is 36°.

Pearce (1983) gives in addition more accurate (but also more complicated) methods which can be used to obtain $\Phi(0/1300)$ values from temperature data. These methods can be extended to obtain values of $\Phi(z/1300)$, the geopotential anomaly between depths z and 1300 m; however, the use of such methods is not further pursued here because of the limited accuracy of the available AXBT measurements. For consistency, equations (1) to (3) are used even when more accurate XBT and CTD pairs are available.

Table 2. Comparisons at site TP6 between barotropic and geostrophic transport estimates, for the strong current at the edge of the meander

Period	Volume transports ($10^6\ m^3\ s^{-1}$)		
	Barotropic	Geostrophic[A]	Ratio
8–15.i.84	63	34 (AX)	1·9
16–23.i.84	57	41 (CTD)	1·4
24–31.i.84	57	37 (AA)	1·5
Average:	59	37	1·6

[A] Geostrophic transports: AA, determination from a pair of AXBT profiles; AX, determination from a combination of AXBT and XBT profiles; CTD, determination from a pair of CTD profiles.

The history of the strong current at the edge of the meander or warm-core ring is known from analysis of detailed weekly charts, compiled from a variety of sources, as described above. The strong current was over site TP6 from 8 to 31 January 1984, and during this time it was straddled by XBT, AXBT and CTD measurements, to give temperature profile pairs on either side. Using the above theory, these pairs of temperature profiles enable three estimates of the geostrophic transport to be made; these are given in Table 2.

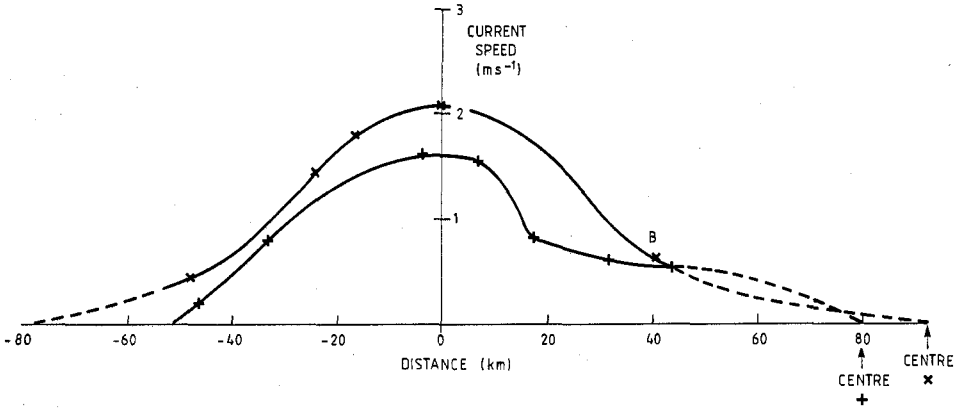

Fig. 6. Surface current speed, obtained from ship-sets, across the strong current at the edge of the meander at two times: × 15 January 1984; + 17–18 January 1984. The zero of distance is set where the current is strongest. The position of the centre of the meander is marked for both times at the right-hand side of the figure. The extra point B is obtained from a satellite-tracked buoy for the time 7–9 January 1984.

To estimate barotropic transport, a current width is needed to combine with barotropic velocity values. For the period 8–31 January 1984, such a current width is estimated from ship-sets observations made by RV *Sprightly*, which crossed the strong current upstream of site TP6 on 15 January, and downstream of site TP6 on 17 to 18 January. For each of these two occasions, the profile of surface current speed across the front is shown in Fig. 6. From each profile in Fig. 6, a 'width of equivalent maximum current' is calculated by dividing the area under the curve by the maximum current value. Widths for 15 January and 17–18 January are thus determined as 69 and 44 km respectively. The average of these two values, 57 km, was taken to apply for the whole period 8–31 January.

The barotropic velocity, based on the sea-floor horizontal electric field data (for site TP6 in this case), is then multiplied by the width of equivalent maximum current and the ocean depth to give an estimate of barotropic transport. This process depends on the assumption that the profile of the strong current at the surface is representative of the profile of the strong current at depth. The process also depends on the evidence that site TP6 was indeed near the maximum of the barotropic flow (otherwise an underestimate of barotropic transport will result).

The barotropic transports thus estimated are 63×10^6 m^3 s^{-1} for 8–15 January and 57×10^6 m^3 s^{-1} for both 16–23 and 24–31 January. These results are also given in Table 2, for comparison with the geostrophic estimates described earlier.

Approximations are involved in obtaining the volume transport values. However, it is evident from Table 2 that the barotropic or total volume transport estimates are consistently greater than those obtained by the normal geostrophic method, by a factor typically of 1·6. The barotropic transport estimates typically exceed the geostrophic transport estimates by an amount of the order of 20×10^6 m^3 s^{-1}.

Such a flow of 20×10^6 m^3 s^{-1} is equivalent to an average velocity throughout the full water depth of approximately 7 cm s^{-1}, for a section of ocean 57 km wide and 5 km

deep. The eastward component of the bottom velocity at site TP6, as given by vertical electric field data (see Fig. 5, and Bindoff *et al.* 1986), is of the order of 2 to 5 cm s^{-1}, and has at times a direction opposite to that of the barotropic component. This particular comparison for site TP6 indicates the existence of a velocity gradient below 1300 m, which may be a normal condition.

Conclusions

The consistency of pattern between the surface, abyssal and barotropic velocity estimates gives some confidence in the general simplicity of the water flow on the scale studied, and in the comparisons drawn between barotropic and geostrophic transport estimates. Although further east (at site TP6) there is some evidence that the bottom velocity is substantially less than the barotropic velocity, near the foot of the continental slope (at site TP9) the bottom and barotropic velocities are often of the same order of magnitude. The suggestion is made, though not developed further in this paper, that the greater barotropic flow near the coast is caused by the deep streamlines converging on the west side of the warm-core ring or meander, due to the proximity of the continental slope.

For the instances studied in the previous section, barotropic transport is greater than geostrophic transport by a factor of approximately 1·6. This result is consistent with the range found from the results of Boland and Hamon (1970) and Hamon (1970), i.e. of 1·2 to 5·0 for the barotropic/geostrophic transport ratio in the Tasman Sea. It appears that the velocity at 1300 m depth for the cases studied (and perhaps typically) is non-zero, and in a similar direction to the near-surface flow. The additional velocity to be added through the water column to account for the barotropic–geostrophic flow differences is of the order of 7 cm s^{-1}.

Mulhearn (1983) demonstrated, with the use of archived data, that strong correlation existed between deep and near-surface perturbations in the East Australian Current region. The present work, in conjunction with that of Mulhearn *et al.* (1986), indicates that the East Australian Current warm-core rings have a very deep structure extending from the surface to abyssal depths. In such cases, transport estimates based on the standard geostrophic techniques clearly give underestimated values. Geostrophic estimates of deep velocities (below approximately 1500 m) are commonly inaccurate; but even though such deep velocities may be small they have a considerable impact on total transport estimates.

Acknowledgments

The deployment and recovery of the sea-floor instruments were carried out from HMAS *Cook*, and the recording current meter was recovered by RV *Sprightly* under charter to CSIRO. The skilful contributions of H. Moeller, G. Pezzoli and T. Koch of Scripps Institution of Oceanography were essential to the experiment. P. M. Tate of the Department of Geology and Geophysics, University of Sydney and L. J. Hamilton of RANRL are thanked for their help with data analysis. J. A. Church of CSIRO is thanked for supplying ancillary data from the Australian Coastal Experiment, and I. S. F. Jones is thanked for helpful sugestions on improving the manuscript, as are two referees.

Scripps Institution of Oceanography and the Australian National University collaborated in the experiment under the US-Australia Agreement for Science and Technology, and US participation was supported in part by US National Science Foundation grants OCE 83-01216 and OCE 83-12399. N.L.B. and I.J.F. were the recipients, respectively, of an Australian Commonwealth Postgraduate Research Award and an Australian National University Research Scholarship.

References

Andrews, J. C., and Scully-Power, P. (1976). The structure of an East Australian Current anticyclonic eddy. *J. Phys. Oceanogr.* **6**, 756–65.

Andrews, J. C., Lawrence, M. W., and Nilsson, C. S. (1980). Observations of the Tasman Front. *J. Phys. Oceanogr.* **10**, 1854–69.

Bindoff, N. L., Filloux, J. H., Mulhearn, P. J., Lilley, F. E. M., and Ferguson, I. J. (1986). Vertical electric field fluctuations at the floor of the Tasman Abyssal Plain. *Deep-Sea Res.* **33**, 587–600.

Boland, F. M., and Church, J. A. (1981). The East Australian Current, 1978. *Deep-Sea Res.* **28**, 937–57.

Boland, F. M., and Hamon, B. V. (1970). The East Australian Current, 1964–1968. *Deep-Sea Res.* **17**, 777–94.

Cresswell, G. R., and Legeckis, R. (1986). Eddies off southeastern Australia. *Deep-Sea Res.* **33**, 1527–62.

Ferguson, I. J., Filloux, J. H., Lilley, F. E. M., Bindoff, N. L., and Mulhearn, P. J. (1985). A sea-floor magnetotelluric sounding in the Tasman Sea. *Geophys. Res. Lett.* **12**, 545–8.

Filloux, J. H. (1980). Observations of very low frequency electromagnetic signals in the ocean. *J. Geomagnetism Geoelectricity* **32**, Suppl. I, S1–S12.

Filloux, J. H., Lilley, F. E. M., Ferguson, I. J., Bindoff, N. L., and Mulhearn, P. J. (1985). The Tasman Project of Seafloor Magnetotelluric Exploration. *Exploration Geophys.* **16**, 221–4.

Godfrey, J. S., Cresswell, G. R., Golding, T. J., Pearce, A. F., and Boyd, R. (1980). The separation of the East Australian Current. *J. Phys. Oceanogr.* **10**, 430–40.

Hamon, B. V. (1965). The East Australian Current, 1960–1964. *Deep-Sea Res.* **12**, 899–921.

Hamon, B. V. (1970). Western boundary currents in the South Pacific. In 'Scientific Exploration of the South Pacific'. (Ed. W. S. Wooster.) pp. 50–9. (Natl Acad. Sci.: Washington, D.C.)

Lilley, F. E. M., Filloux, J. H., Bindoff, N. L., Ferguson, I. J., and Mulhearn, P. J. (1986*a*). Barotropic flow of a warm-core ring from seafloor electric measurements. *J. Geophys. Res.* **91**, 12979–84, 13109.

Lilley, F. E. M., Mulhearn, P. J., Filloux, J. H., Bindoff, N. L., and Ferguson, I. J. (1986*b*). Pressure fluctuations on the open-ocean floor: mid Tasman Sea at 38°30′S.,162°38′E., near the Lord Howe rise. *Aust. J. Mar. Freshwater Res.* **37**, 27–37.

Mulhearn, P. J. (1983). Deep currents of the northern Tasman Sea Basin. *Deep-Sea Res.* **30**, 1119–26.

Mulhearn, P. J., Filloux, J. H., Lilley, F. E. M., Bindoff, N. L., and Ferguson, I. J. (1986). Abyssal currents during the formation and passage of a warm-core ring in the East Australian Current. *Deep-Sea Res.* **33**, 1563–76.

Nilsson, C. S., and Cresswell, G. R. (1981). The formation and evolution of East Australian Current warm-core eddies. *Prog. Oceanogr.* **9**, 133–83.

Pearce, A. F. (1983). Estimation of dynamic heights from temperature profiles in the Tasman Sea. *Aust. J. Mar. Freshwater Res.* **34**, 115–19.

Manuscript received 27 July 1987, revised 1 September 1988, accepted 19 September 1988